Catalysis Communications 11 (2009) 240–246

Contents lists available at ScienceDirect

Catalysis Communications

journal homepage: www.elsevier.com/locate/catcom

Effect of MgO addition on the basicity of Ni/ZrO_2 and on its catalytic activity in carbon dioxide reforming of methane

Verónica García, Jhon J. Fernández, Wilson Ruíz, Fanor Mondragón, Andrés Moreno *

Institute of Chemistry, University of Antioquia, A.A. 1226, Medellín, Colombia

ARTICLE INFO

Article history:
Received 17 April 2009
Received in revised form 10 September 2009
Accepted 5 October 2009
Available online 13 October 2009

Keywords:
Methane reforming
Magnesia-stabilized zirconia
Ni/ZrO_2 catalyst
Activation energy of CO_2 desorption

ABSTRACT

The effect of the MgO content on the basicity and on the catalytic performance of Ni/ZrO_2–MgO catalysts for carbon dioxide reforming of methane was studied. MgO addition to the zirconia support by co-precipitation (5% MgO) had several effects: stabilized the zirconia tetragonal phase by increasing its thermal stability, increased the basicity of the support, and decreased the reducibility of Ni^{2+}. The CO_2 desorption energy distribution functions calculated from the TPD-CO_2 profiles were centred at activation energies around 100–134 kJ mol^{-1}. Besides the effect due to the modification of the zirconia properties by MgO addition, the catalytic activity was also related to the reduction degree of nickel on Ni/ZrO_2–MgO catalysts, while the catalyst stability was related to the basic properties of the supports.

1. Introduction

The transformation of light hydrocarbons is a challenge of practical and theoretical interest, particularly the efficient use of the methane, the main component of the natural gas, is an important objective due to the existence of large deposits and to the progressive diminution of the traditional fuel source (petroleum). The indirect conversion of methane into other compounds is usually performed via syngas formation over metal catalysts. Syngas (H_2–CO mixture) is mainly produced by steam reforming of methane [1] by the following reaction:

$$CH_4 + H_2O \rightarrow CO + 3H_2 \quad \Delta H^{\circ}_{25^{\circ}C} = +206 \text{ kJ mol}^{-1} \tag{1}$$

Although steam reforming of methane is commercially applied to produce syngas (a mixture of H_2 and CO), lower ratios are needed for oxo- and Fischer–Tropsch synthesis. The methane reforming reaction with carbon dioxide, also known as dry reforming (reaction (2)), constitutes an attractive alternative due to its high selectivity towards carbon monoxide, useful in the long chain hydrocarbon [2] and oxygenates derivatives synthesis [3]. Furthermore, this process is of great interest for environmental issues since the reaction consumes two important greenhouse gases (CH_4 and CO_2) to convert them into valuable feedstock and also to increase the valorization of gas-field with high carbon dioxide content.

$$CH_4 + CO_2 \rightarrow 2CO + 2H_2 \quad \Delta H^{\circ}_{25^{\circ}C} = +247 \text{ kJ mol}^{-1} \tag{2}$$

One of the major problems of CH_4–CO_2 reforming is the high thermodynamic potential to coke formation by the following two reactions:

$$CH_4 \rightarrow C + 2H_2 \quad \Delta H^{\circ}_{25^{\circ}C} = +75 \text{ kJ mol}^{-1} \tag{3}$$

$$2CO \rightarrow C + CO_2 \quad \Delta H^{\circ}_{25^{\circ}C} = -173 \text{ kJ mol}^{-1} \tag{4}$$

These reactions are favored at high and at low temperatures, respectively. Thus, from the practical viewpoint, it is preferable to operate CO_2 reforming of methane at moderate temperatures, which requires a catalyst that kinetically inhibits the carbon formation under the conditions that are thermodynamically favorable for carbon deposition.

Moreover, considering the dry reforming of methane is influenced by the simultaneous occurrence of RWGS (Reverse of Water Gas-Shift) reaction; indeed, it is frequently found that CH_4 conversion is lower than CO_2 conversion, according with reaction (5):

$$CO + H_2O \rightarrow CO_2 + H_2 \quad \Delta H^{\circ}_{25^{\circ}C} = -41 \text{ kJ mol}^{-1} \tag{5}$$

Currently the commercial implementation of dry reforming is hindered by the absence of suitable inexpensive catalysts that provide high activity, selectivity and stabilility. Numerous investigations on catalyst development for the dry reforming have been reported [4–8]. Although noble metals have been successfully used in terms of activity and selectivity [9,10], the cost and limited availability have discouraged their industrial application. Nickel-based catalysts have been employed as possible substitute for noble metals, as they are relatively cheap and are known to possess high activity [11–13]. However, studies have shown that

* Corresponding author.
E-mail address: jamoreno@matematicas.udea.edu.co (A. Moreno).

1566-7367/$ - see front matter © 2009 Elsevier B.V. All rights reserved.
doi:10.1016/j.catcom.2009.10.003

nickel is more susceptible to coking and deactivation [2,14], therefore the search for suitable new catalysts is still a priority. In this sense, one of the current trends in this field concerns the improvement of the metal dispersion by using as catalyst solid precursors containing active metals like hydrotalcites, perovskites and solid solutions (NiO–MgO) [8,15,16]. Another line of research is the study of bimetallic systems [17] and the addition of promoters (basic or redox oxides) [18–21]. It is known that the use of a basic support [5] favours CO_2 adsorption and its dissociation, which contributes to gasify the carbonaceous deposits and to decrease the deactivation by coke formation. Nevertheless, it has been also found that the addition of these basic oxides reduces not only the formation of coke but also the rate of the reforming reaction [22].

Zirconium oxide has been widely applied as catalytic support for different reactions due to its high thermal stability and unique chemical (redox and acid–base) properties [23,24]; on the other hand, it has been reported that Ni/ZrO_2 catalyst deactivates due to coke formation and by sintering during dry reforming of methane. In order to increase catalyst stability, several research works concerning zirconia-based catalysts modified with different oxides (e.g., CaO, MgO, CeO_2) have been reported [25–27]. An improved nickel dispersion and enhanced interaction between CO_2 and the catalyst during the dry reforming of methane were observed when magnesium is added as promoter [26]. The addition of CaO to the zirconium oxide forms a solid solution, decreasing the reduction temperature of supported nickel and reducing coke accumulation during methane conversion [18].

The objective of the present work was to study the effect of the MgO addition on the basicity and on the catalytic performance of Ni/ZrO_2 catalysts for the carbon dioxide reforming of methane. The surface basicity of the supports and catalysts was studied by temperature-programmed desorption of CO_2 (CO_2-TPD) and the activation energy of desorption was calculated from the CO_2-TPD profiles. The reducibility of the supported Ni^{2+} was studied by temperature-programmed reduction (TPR).

2. Experimental

2.1. Catalysts preparation

The catalysts were prepared by wet impregnation of an aqueous solution of Ni^{2+} onto zirconia supports containing variable nominal MgO amounts (1–5 wt.%). ZrO_2–MgO supports were prepared by co-precipitation method at constant pH (pH 9–10) by drop-wise addition of a mixed solution of the cations (Zr^{4+} and Mg^{2+}) to a concentrated ammonia aqueous solution (28 wt.%). The oven-dried mixed hydroxides were pre-calcined at 500 °C for 3 h in static air. This pre-calcination step was performed in order to facilitate the solid state reaction between zirconium and magnesium hydroxides and to avoid a possible redissolution of MgO during the wet impregnation with Ni^{2+} solution. After impregnation and drying at 100 °C, the solids were calcined in static air for 3 h at 700 °C, with temperature linearly increased at a rate of 5 °C min^{-1}.

2.2. Catalysts characterization

The Ni^{2+} and Mg^{2+} contents of the calcined catalysts were determined by atomic absorption spectroscopy. Thermal stability of different catalysts was evaluated by thermogravimetric analysis using a TGA 2950 thermo-analyser (TA Instruments) from 25 °C to 950 °C in air flow (10 °C min^{-1}, 100 mL min^{-1}). Specific surface areas of the different solids were determined by N_2 adsorption at −196 °C in an ASAP 2000 system (Micromeritics), and applying the BET model. Prior to the analyses the solids were outgassed for 24 h at 120 °C under vacuum.

X-ray diffraction was used to determine the crystal structure of the solids. Samples in the powder form were analyzed in a Kristalloflex D-5000 (Siemens) difractometer (Cu Kα radiation, $\lambda = 1.5418$ Å, 40 kV, 30 mA) at a scanning rate of 0.03° 2θ every 5 s.

XPS analysis of the solids was performed with an SSI X-Probe (SSX-100/206) photoelectron spectrometer equipped with a monochromatized microfocus Al X-ray source. The sample powder pressed in a small stainless steel troughs of 4 mm diameter were placed on an aluminum carousel. Zr 3d, Mg 2s, Ni 2p, O 1s and C 1s signals were measured. The binding energy (BE) reference was taken at the C 1s peak from carbon contamination of the samples at 284.8 eV. The atomic concentration ratios were calculated from the peak areas normalized on the basis of acquisition parameters and sensitivity factors provided by the manufacturer.

The reducibility of the calcined catalysts (NiO_x/ZrO_2–MgO) was studied by temperature-programmed reduction (TPR) in a chemisorption unit (AutoChem 2910, Micromeritics). The samples (50 mg) were treated at 500 °C in He flow, and after cooling to 25 °C, a TPR was run under a 5% H_2/Ar gas mixture from 25 to 900 °C (10 °C min^{-1}, 50 mL min^{-1}). The consumption of hydrogen was monitored on-line with a thermal conductivity detector.

The supports and catalysts basic surface properties were determined by temperature-programmed desorption of carbon dioxide (TPD-CO_2). The measurements were carried out in a quartz micro-reactor using He as carrier gas. Prior to the adsorption of CO_2, the samples (100 mg) were pre-treated at 500 °C for 1 h (100 mL min^{-1}) for cleaning the surface from moisture and other adsorbed gases. In order to evaluate the basicity over reduced catalysts, the Ni^{2+}-containing solids were further treated with 5% H_2 in Helium gas mixture (100 mL min^{-1}) at 500 °C for 1.5 h. After cooling at 50 °C the samples were saturated by passing a stream of 5% CO_2 in Helium (100 mL min^{-1}) for 30 min, then the gas mixture was changed to He to purge the gas line and to remove weakly adsorbed CO_2. After 1 h purge, temperature was raised at 10 °C min^{-1} from 50 °C to 700 °C under He flow (100 mL min^{-1}). Carbon dioxide desorbed from the sample was on-line monitored with a quadrupole-type mass spectrometer (Thermo Onix, ProLab300). The desorption profiles presented here are the signal of the $m/z = 44$, corresponding to CO_2 species. The quantitative analysis of desorbed CO_2 was done by integration of the area of the desorption profile, which was calibrated using the CO_2 produced in the decomposition of $MgCO_3$ (Merck). The distribution function of the CO_2 desorption activation energy from supports and catalysts treated with mixture of CO_2/He at 50 °C, was determined. The algorithm employed in the calculation was a variation of the stochastic method commonly used for the evaluation of the activation energies from TPD data, which described the TPD process as the desorption of a series of surface complexes with different activation energies [28].

2.3. Catalytic activity measurements

The CO_2 reforming of methane was carried out in a fixed-bed quartz micro-reactor (11 mm i.d.) operated at atmospheric pressure and 600 °C. The reaction temperature was controlled with the aid of a thermocouple located externally to the catalyst bed. Prior to the introduction of the feed (1 CH_4 : 1 CO_2 : 2 He; total flow 200 mL min^{-1}), the catalysts (50 mg) were reduced at 500 °C for 1.5 h (10% H_2 in He; 100 mL min^{-1}). After removing the water produced during the reaction (via water–gas shift reaction) using silica gel, the reaction products were analyzed on-line by gas chromatography (Shimadzu GC-9A), with a thermal conductivity detector and a 3 m Carbosieve S II packed column.

3. Results and discussion

3.1. Physico-chemical properties of supports and catalysts

The characterization results of the chemical analyses and specific surface areas of the supports and calcined catalysts (700 °C) are presented in Table 1. The chemical analysis results indicate that for all samples the nickel content was close to the nominal values (10 wt.%) introduced during the impregnation step in the catalysts preparation. Also from Table 1, it is observed that there is a correlation between the MgO content obtained by chemical analysis and the nominal MgO loading introduced during the co-precipitation. However, it should be pointed out that the MgO contents differ considerably from the expected values according to the synthesis procedure. This indicates that nearly 60% of the Mg^{2+} did not precipitate upon addition of the mixed Zr^{4+}–Mg^{2+} solution to the concentrated ammonia solution. This result is not surprising if one considers the solubility product constant of the magnesium hydroxide ($K_{sp} = 5.61 \times 10^{-12}$), which means that a pH higher than 10 is required for the quantitative precipitation of the Mg^{2+}. In the present work, ammonia was selected as precipitating agent in order to avoid the risk of contamination of the precipitate with counter-ions usually present when other common precipitating chemicals are used (i.e., NaOH). The synthesis procedure adopted allowed us to get solids with variable MgO content, which was a parameter studied in the present work.

From Table 1, it is also observed that at 500 °C the Mg^{2+}-containing supports showed a higher surface area than zirconium oxide. However, this effect becomes less important when solids are calcined at a higher temperature (i.e., 700 °C); the catalysts calcined at 700 °C have a specific surface area around to 25 $m^2\ g^{-1}$.

Two typical 2θ peaks at 28.3° and 31.5° 2θ ascribed to the monoclinic zirconia phase are observed in the XRD profile for the pure zirconia sample calcined at 700 °C (Fig. 1a), while for the sample modified with 2.3 wt.% MgO, the tetragonal zirconia phase (t-ZrO_2) is predominant (with main diffraction lines at 30.4° and 50.8° 2θ). These X-ray diffraction results indicated that the addition of Mg^{2+} increased the thermal stability of the zirconia support. Montoya et al. [25] suggested that MgO stabilizes the t-ZrO_2 by incorporating in the surface vacancies or covering the particles and preventing the contact between the crystallites of (t-ZrO_2) avoiding the crystallite growth and the tetragonal to monoclinic transformation. Stefanic et al. [29] attributed the tetragonal and cubic stabilization at room temperature to the addition of different oxides, *viz.* MgO, CaO, Sc_2O_3, Y_2O_3. The main effect, due to the formation of a solid solution, is the decrease in the Zr coordination number by the introduction of oxygen vacancies associated with the lower charge of the guest cations.

3.2. Temperature-programmed reduction (TPR) of supported Ni^{2+}

Fig. 2 shows the reduction profiles (TPR) of the calcined catalysts with variable MgO content. Under the same experimental conditions, bulk NiO (Aldrich) showed a single symmetric peak centred at 363 °C, which can be ascribed to the reduction of Ni^{2+} to nickel Ni°. When Ni^{2+} is supported over the zirconium oxide (NiO/ZrO_2) two reduction peaks at 430 and 570 °C were observed. Consistent with this observation, for Ni/ZrO_2 catalysts prepared by impregnation (melt-salt method), Roh et al. observed a wide band with maxima at 400 and 510 °C [30], while Montoya et al. observed a single peak at 548 °C, for zirconia-based catalysts, in which the Ni^{2+} was introduced by co-precipitation (via sol–gel method) [31].

Our results suggest the existence of two different NiO species on the zirconia surface; the high temperature peak can be ascribed to NiO_x species strongly interacting with the ZrO_2 surface (i.e.,

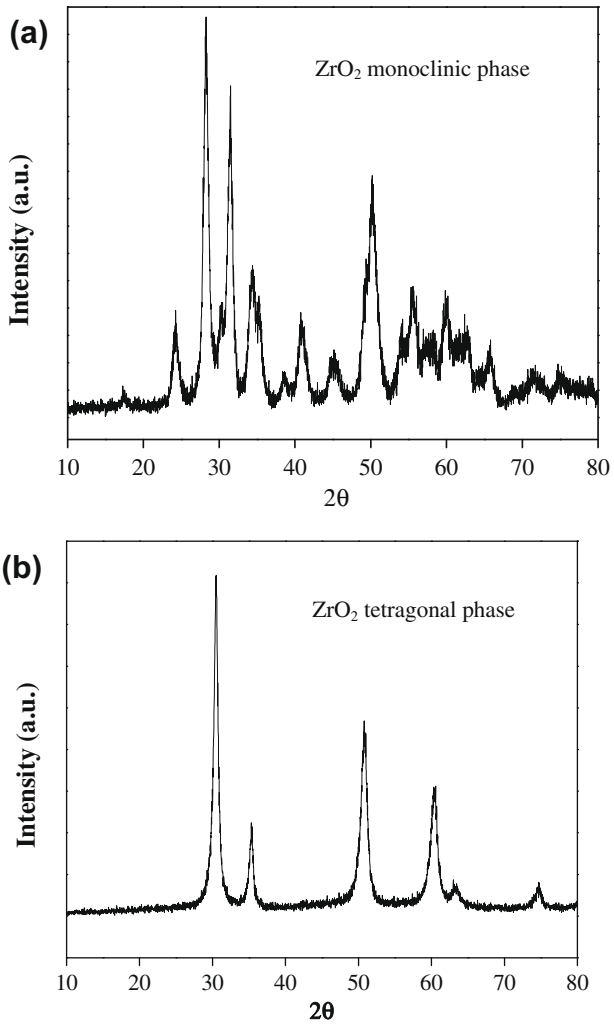

Fig. 1. XRD patterns of the supports after calcination at 700 °C (a) ZrO_2 and (b) ZrO_2–2.3% MgO.

Table 1
Chemical analysis and surface area results for supports and non-reduced calcined at 700 °C.

Supports			Non-reduced catalysts calcined at 700 °C (NiO/ZrO_2–MgO)			
Sample	S_{BET} ($m^2\ g^{-1}$)		Sample	S_{BET}	Ni[a]	MgO[b]
Calcn. Temp.	500 °C	700 °C		($m^2\ g^{-1}$)	(%)	(%)
ZrO_2	72	37	NiO/ZrO_2	26	–	0.0
ZrO_2–1% MgO	91	29	NiO/ZrO_2–1% MgO	n.d.	9.4	0.4
ZrO_2–3% MgO	n.d.	n.d.	NiO/ZrO_2–3% MgO	18	10.5	1.2
ZrO_2–5% MgO	112	21	NiO/ZrO_2–5% MgO	23	10.1	2.3

[a] Nominal 10 wt.% with respect to the reduced catalyst (Ni/ZrO_2–MgO).
[b] Nominal values 0, 1, 3, 5 wt.%, with respect to the ZrO_2–MgO support.

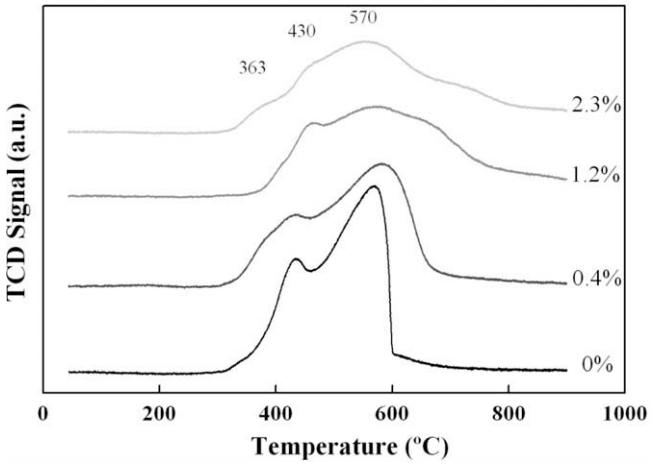

Fig. 2. H_2-TPR profiles for non-reduced catalysts Ni/ZrO_2–MgO with increasing MgO content (0–2.3% MgO).

direct contact), while the low temperature peak would probably be due to the reduction of NiO_x species, which are not in direct contact with the ZrO_2 surface, accordingly, the reduction peak appeared at lower temperature. It could not be ruled out that the two peaks observed were related to NiO particles interacting with different surface ambient on the zirconia support (i.e., steps, kinks, etc.); however, our results did not could give evidence to proof this hypothesis.

It could also be seen in Fig. 2 that reduction peaks shifted to higher temperatures with increasing the MgO content, and they become complex (wider peaks), suggesting an increasing Ni^{2+}-support interaction, and probably providing evidence about the heterogeneity of the catalysts surface. In addition, there is a low reduction shoulder-like peak near 360 °C for both 0.4% and 2.3% MgO samples, which could be ascribed to NiO crystallites; although it is not clear why the solid with an intermediate magnesia content (i.e., 1.2% MgO) did not showed this peak, this observation further confirms the comment above concerning the heterogeneity of the catalysts surface. The observed shift of the reduction peak to higher temperatures could be ascribed to the increasing number of interacting Ni^{2+}–O–Mg^{2+} sites due to the progressive increasing of the MgO content in the support. It is well known that for Ni/MgO catalysts (abundant Ni^{2+}–O–Mg^{2+} sites), the reduction of Ni^{2+} (i.e., NiO) occurs at relatively high temperatures (ca 800–850 °C) [32].

3.3. XPS

The XPS was used to obtain further information about the surface composition of ZrO_2–MgO supports and NiO/ZrO_2–MgO catalysts by inspecting the spectral line shape and intensities of the Zr3d, Mg2s, and Ni2p and O1s core-level electrons.

The Mg/Zr ratio for the supports increased with the Mg content from 0.4 to 2.3 wt.% MgO (Table 2). For the calcined catalysts NiO/ZrO_2–MgO, the Mg/Zr ratio was about one order or magnitude higher than that in supports (ZrO_2–MgO), indicating that the NiO presence enhances the Mg^{2+} surface concentration and suggest a strong NiO–MgO interaction. To obtain information about structural differences for ZrO_2–MgO supports, the XPS spectra in the O1s binding energy (BE) was determined, (Fig. 3). Mixed oxides exhibit two peaks: one at 529.8 eV corresponding to O^{2-} lattice ions, and the other at and 531 eV assigned to oxygen containing species like hydroxyl and carbonate groups [33]. The presence of surface carbonates is also confirmed by the C1s peak at ca. 289 eV. For pure MgO support the O^{2-} lattice peak component is not observed, probably due to the higher content of the carbonate and/or hydroxyl species at the surface. Ardizzone et al. [34] found that the affinity between the surface chemisorbed –OH and MgO is so strong that a fraction of them remains even after a treatment at a temperature as high as1200 °C.

The O1s spectra for NiO/ZrO_2 and NiO/MgO catalysts are presented in Fig. 4. As in the case of the supports, two different oxygen components are observed at 529.5 eV and 531.5 eV. The intensity of O1s signal at 531.5 eV over NiO/MgO, associated with hydroxyl and/or carbonate species at the surface, is much higher than that over NiO/ZrO_2, implying the higher basicity of oxygen surface on

Table 2
Mg/Zr ratio obtained by XPS for zirconia –magnesia supports and calcined catalysts (Mg2s and Zr3d).

Sample %MgO	ZrO_2–MgO Mg/Zr	NiO/ZrO_2–MgO Mg/Zr
0.4	0.05	0.43
1.2	0.11	1.28
2.3	0.15	2.33

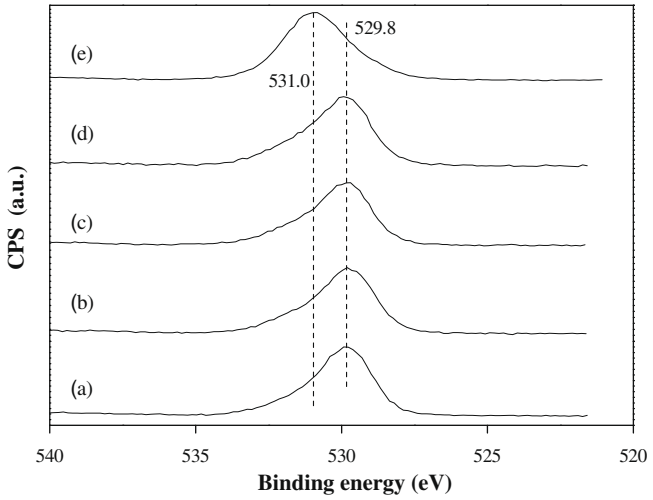

Fig. 3. O1s XPS spectra of (a) ZrO_2, (b) ZrO_2–0.4% MgO, (c) ZrO_2–1.2% MgO, (d) ZrO_2–2.3% MgO and (e) MgO.

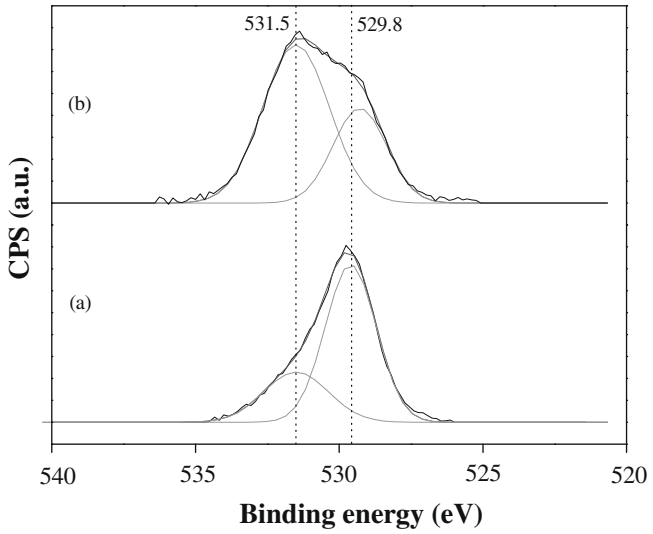

Fig. 4. O1s XPS spectra of (a) NiO/ZrO_2 and (b) NiO/MgO.

NiO/MgO than NiO/ZrO_2. In addition, the complexity of O1s signal on NiO/MgO surface relative to NiO/ZrO_2, constitutes an evidence of the strong interaction NiO/MgO (see TPR results).

3.4. Temperature-programmed desorption of CO_2

3.4.1. TPD-CO_2 profiles

Fig. 5 shows the CO_2 desorption profiles obtained for zirconia–magnesia supports with increasing MgO content. It can be seen that zirconia support has a desorption peak with a maximum at 110 °C, which is slightly shifted to higher temperatures with increasing the MgO content. Moreover, the TPD profile is highly asymmetric with desorption curve extending up to 300 °C. For the MgO support the desorption peak appeared at about 147 °C, along with a shoulder at 260 °C. Since basic sites are classified according to their different strength (different CO_2 desorption temperature), the results in Fig. 5 indicate that the addition of Mg^{2+} to zirconium oxide induces only a slight increase of the strength of the basic sites, and introduces new basic sites (additional shoulder at 260 °C) to zirconia, likely associated to the Mg–O sites.

The ZrO_2–MgO (0.4%) support has a similar profile to zirconia, a desorption peak at 119 °C, followed by a small shoulder at 190 °C. The ZrO_2–MgO (2.3%) support has a similar peak, now at 124 °C, and as for MgO, a shoulder at higher temperature (ca. 213 °C) with respect to that observed for ZrO_2–MgO (0.4%) support. The amount of CO_2 desorbed, calculated from the integration area of desorption profiles and normalized by the surface area, are presented in Table 3. From these data, it can be concluded that the Mg^{2+}-containing supports have an increased number of basic sites (higher amount of desorbed CO_2) with respect to the zirconia support. It is worth mentioning that a small addition of Mg^{2+} (0.4 wt.% MgO) increased the number of basic sites by a factor of two. In the present work, Mg-containing zirconias showed higher amount of basic sites compared to the single oxides. Similar results over magnesia–zirconia oxides were reported by Aramendía et al. [35].

CO_2-TPD curves for the reduced Ni/ZrO_2 and zirconia support, presented in Fig. 6a, show that the profile and the intensity is similar to that of ZrO_2. A comparison of the amount of CO_2 desorbed from Ni/ZrO_2 and ZrO_2 (Table 3) suggests that nickel impregnation does not affect (increase or reduce) the number of basic sites responsible for the CO_2 adsorption. As shown in Fig. 6b, for Ni/ZrO_2–MgO (2.3%) catalyst, similar results were obtained for the catalysts containing Mg^{2+}, i.e., there were no important differences on the amount of CO_2 desorbed between the supports and the reduced catalysts. If it is assumed that the CO_2 adsorption occurred on Mg–O sites at the surface, this result would be contrary to what it would be expected according to the XPS results over calcined

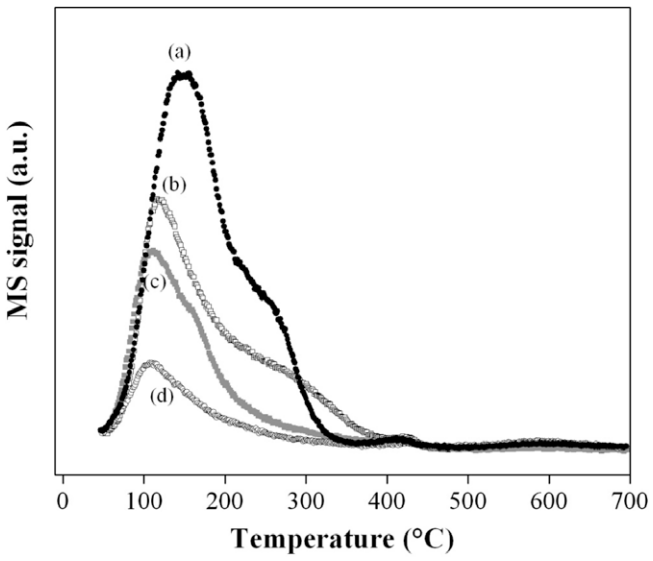

Fig. 5. CO_2-TPD of (a) MgO, (b) ZrO_2–2.3% MgO, (c) ZrO_2–0.4% MgO and (d) ZrO_2.

Table 3
CO_2 desorbed during the CO_2-TPD over supports and Ni/ZrO_2 catalyst and activation energy of CO_2 desorption.

Sample	μmol CO_2/m^2	Activation energy (kJ mol^{-1})	
		Ea_1	Ea_2
MgO	2.4	109.5	134.0
ZrO_2–2.3wt.% MgO	4.3	104.2	127.0
ZrO_2–0.4wt.% MgO	2.3	104.2	121.8
ZrO_2	1.0	100.5	115.9
Ni/ZrO_2	1.5[a]	n.d.	n.d.

[a] Based on the surface area of non-calcined catalyst.

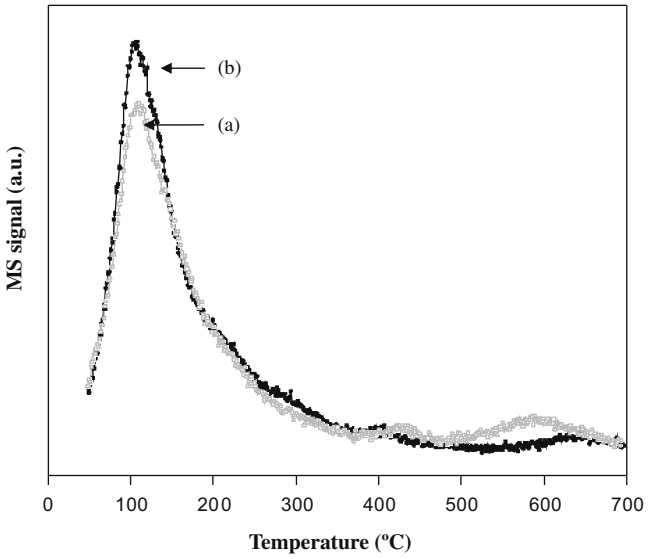

Fig. 6a. CO_2-TPD of zirconium catalyst and support (a) Ni/ZrO_2 and (b) ZrO_2.

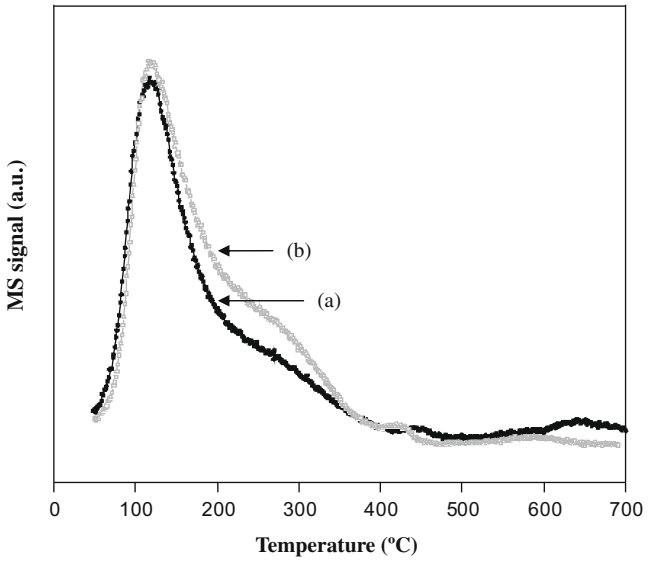

Fig. 6b. CO_2-TPD of zirconium–magnesia (2.3 wt.% MgO) catalyst and support (a) Ni/ZrO_2–2.3% MgO and (b) ZrO_2–2.3% MgO.

NiO/ZrO_2–MgO catalysts indicating a surface enrichment with Mg^{2+}. The similar CO_2 adsorption over supports and Ni-supported reduced catalysts suggest that, due to the strong interaction between NiO and MgO, impregnation with nickel induced a migration of the Mg^{2+} to the surface and not necessarily increased the basicity of the solids. This hypothesis is in agreement to the TPR results which indicated that reduction of NiO is affected by the presence of Mg^{2+}.

It could be concluded that the CO_2 is mainly adsorbed on Zr–O and Zr–O–Mg sites at the surface of the support on reduced catalysts, as reported for Ni/MgO catalyst [36]. Furthermore, the CO formation during the TPD-CO_2 is not important and then the dissociative CO_2 adsorption is neglected.

3.4.2. Desorption activation energy and its distribution function

The calculated energy distribution functions, assumed as a combination of two normal Gaussians distribution functions, were centred at activation energies around 100–134 kJ mol^{-1} (Fig. 7); accordingly, two maxima of the activation energy of desorption (Ea_1 and Ea_2) were obtained. The results in Table 3 are in agreement with activation desorption energy results reported by Bachiller et al. [37] for ZrO_2 (97–130 kJ/mol) and Auroux et al. [38] for MgO (110 kJ/mol).

There is a narrow distribution of the sites with the lower desorption activation energy (Ea_1, Table 3) with respect to the sites desorbing CO_2 at higher temperature (Ea_2), as shown in Fig. 7. For ZrO_2 the population of sites with lower activation energy of CO_2 desorption is much larger than those with higher desorption activation energy. In the case of MgO the population sites with Ea_1 was larger than those with Ea_2. The addition of MgO increased the population of the sites with the high desorption activation energy at expense of the sites with lower desorption Ea; in other words, the addition of MgO to the zirconia support increased the strength of the basic sites at the surface of the solids. As will be shown in the next section, the increase of the strength of the basic sites seems to be responsible for the higher stability of the MgO-containing catalysts, due to the ability of the support to chemisorb CO_2, which would contribute to the gasification of the carbonaceous species being formed at the surface of the catalysts, as confirmed by the amount of coke measured after reaction.

3.5. Catalytic activity

Fig. 8a shows the curves of the methane conversion with time at 600 °C for the catalysts with different MgO content. At the reaction conditions adopted, Ni-free supports (ZrO_2 and ZrO_2–MgO) were not active; Ni/ZrO_2 catalyst shows a progressive deactivation with time, and deactivation was slightly less pronounced for Mg^{2+}-containing catalysts, and all of them exhibited a relatively stable regime of conversion above 100 min of reaction. All of these results were reproducible. In the case of the catalyst containing 0.4 wt.% MgO, the methane conversion remains practically constant in time, after 5 h of continuous reaction it became the most stable catalyst.

Similar reaction profiles were observed for the conversion of carbon dioxide (Fig. 8b). On the other hand, for all catalysts it was found that the carbon dioxide conversion was superior to that of the methane. The carbon balance for these reactions was about 95%. The observed differences between the CO_2 and the CH_4 conversion suggest that besides the reforming reaction, an additional fraction of the carbon dioxide was consumed according to the reverse water–gas shift reaction [3], indeed, formation of water was also detected in the moisture trap located at the exit of the reactor. Although our experimental setup did not allow simultaneously measuring H_2 and CO, due to the low sensibility of the

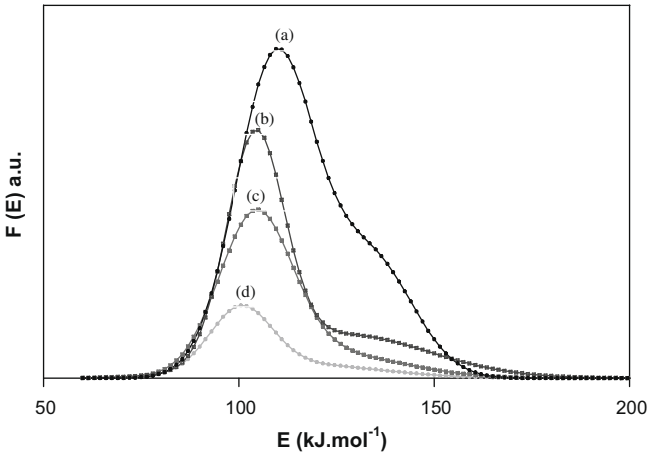

Fig. 7. Energy distribution functions obtained from the CO_2 desorption profile of ZrO_2–MgO supports (a) MgO, (b) ZrO_2–2.3% MgO, (c) ZrO_2–0.4% MgO and (d) ZrO_2.

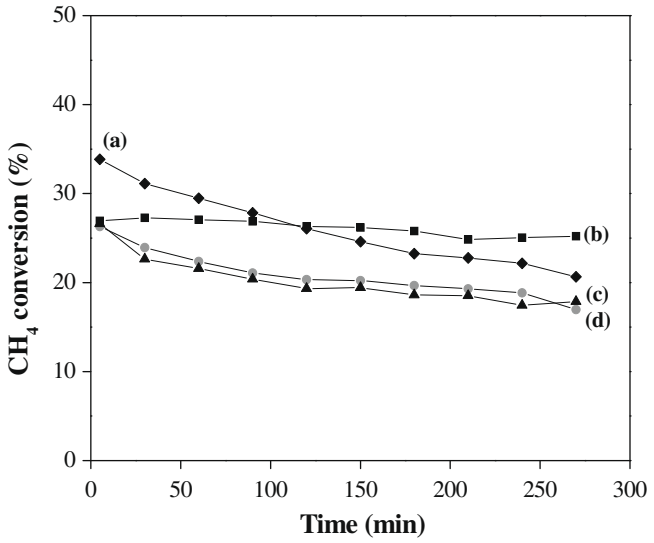

Fig. 8a. Methane conversion vs. time using Ni/ZrO_2–MgO catalysts at 600 °C (a) Ni/ZrO_2, (b) Ni/ZrO_2–0.4% MgO, (c) Ni/ZrO_2–1.2% MgO and (d) Ni/ZrO_2–2.3% MgO.

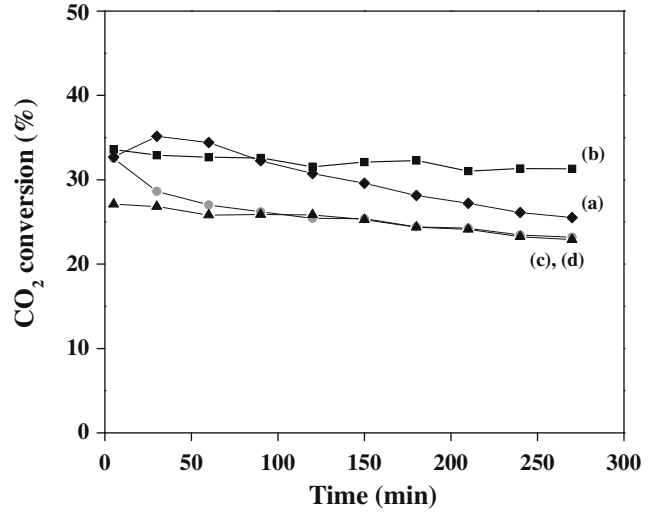

Fig. 8b. CO_2 conversion vs. time using Ni/ZrO_2–MgO catalysts at 600 °C (a) Ni/ZrO_2, (b) Ni/ZrO_2–0.4% MgO, (c) Ni/ZrO_2–1.2% MgO and (d) Ni/ZrO_2–2.3% MgO.

Table 4
Amount of carbonaceous residues after 5 h reaction at 600 °C.

Catalyst	mg C/mg catal.
Ni/ZrO_2	0.80
Ni/ZrO_2–0.4% MgO	0.26
Ni/ZrO_2–1.2% MgO	0.31
Ni/ZrO_2–2.3% MgO	0.26

TCD when using He as carrier gas, from the results in Figs. 8a and b it is clear that the H_2/CO ratio should be lower than 1, and it could be likely near to 0.8, as it was recently observed over $Ni/CaO–ZrO_2$ catalysts [39].

For $Ni//ZrO_2$–MgO catalysts containing 1, 8 and 20 wt.% MgO, Montoya et al. [25] observed that the catalyst with 1 wt.% MgO showed the highest conversion, selectivity and stability; these authors suggested that the better catalytic activity of this solid was due to the pore active Ni crystallites-support interfaces sites created on the surface after reduction. Our catalysis results are consistent with this hypothesis, furthermore the XPS results confirms that upon impregnation with nickel Mg^{2+} migrate from the bulk of ZrO_2 tetragonal phase during calcination to the surface which could react with NiO forming a solid solution as in the case of Ni/MgO catalyst [4]. The formation of this Ni-support interface sites would be favoured with the lowest MgO content.

Previous research has shown that methane is mainly activated over the metallic sites on the catalyst (i.e., Ni°) [3]. On the other hand, the results from H_2-TPR indicated that the reducibility of the Ni^{2+} decreased with the increase of the magnesium content; this is probably due to the fact that the strong interactions between Ni and Mg makes the catalysts less reducible, and therefore reduces the activity for the reforming reaction. The progressive deactivation observed for the catalyst without Mg^{2+} (i.e., Ni/ZrO_2) suggests that in the absence of magnesium a higher fraction of reduced nickel could be obtained, being then more favourable the conversion of methane, over the Ni° sites, to other products (such as coke precursors), by a reaction path different to the reforming reaction. In agreement with this hypothesis the analysis of coke by TGA (see Table 4) show that after 5 h of reaction at 600 °C, the formation of a carbonaceous residue on the surface of the catalyst was appreciably lower for Mg^{2+}-containing catalysts as compared to the Mg^{2+}-free catalyst (Ni/ZrO_2).

4. Conclusions

The addition of Mg^{2+}, via co-precipitation, to zirconia increased its thermal stability by inhibiting the transformation of the tetragonal metastable phase to monoclinic phase. Furthermore, the presence of Mg^{2+} shifted the reduction of the Ni^{2+} to higher temperatures for the Ni/ZrO_2–MgO catalysts. In the absence of Mg^{2+}, Ni^{2+} could be reduced at lower temperature. The addition of MgO to Ni/ZrO_2 prevents the deactivation of the catalyst by combination of the increase of basic properties on the surface of the support and the strong metal support interaction of Ni/ZrO_2–MgO catalysts.

Acknowledgements

The authors acknowledge to the University of Antioquia for the financial support (project IN521CE, CODI-2003), and the Sostenibilidad program 2009–2010. V. García thanks Colciencias and the University of Antioquia for her Ph.D. scholarship. The authors thank Laboratoire de Catalyse en Chimie Organique (Université de Poitiers) for assisting with the TPR analysis and Unité de Catalyse et Chimie des Matériaux Divisés (Université catholique de Louvain UCL) for XPS facilities.

References

[1] A.P.E. York, T.-C. Xiao, M.L.H. Green, J.B. Claridge, Catal. Rev. Sci. Eng. 49 (2007) 511.
[2] A.M. Gadalla, B. Bower, Chem. Eng. Sci. 43 (1988) 3049.
[3] M.C.J. Bradford, M.A. Vannice, Catal. Rev. Sci. Eng. 41 (1999) 1.
[4] E. Ruckenstein, Y.H. Hu, J. Catal. 161 (1996) 55.
[5] J.H. Bitter, K. Seshan, J.A. Lercher, J. Catal. 171 (1997) 279.
[6] R. Rostrup-Nielsen, Catal. Rev. Sci. Technol. 46 (2004) 247.
[7] A. Djaidja, S. Libs, A. Kiennemann, A. Barama, Catal. Today 113 (2006) 194.
[8] G. Sierra, F. Mondragón, J. Barrault, J.-M. Tatibouët, C. Batiot-Dupeyrat, Appl. Catal. A: Gen. 311 (2006) 164.
[9] J.R. Rostrup-Nielsen, J.H.B. Hansen, J. Catal. 144 (1993) 38.
[10] F. Solymosi, G. Kutsan, A. Erdohelyi, Catal. Lett. 11 (1991) 149.
[11] Z. Zhang, X.E. Verykios, Appl. Catal. A: Gen. 138 (1996) 109.
[12] S. Wang, G.Q. Lu, Appl. Catal. B: Environ. 16 (1998) 269.
[13] G.Q.M. Lu, S. Wang, Chemtech 29 (1999) 37.
[14] A.T. Ashcroft, A.K. Cheetham, M.L.H. Green, P.D.F. Vernon, Nature 352 (1991) 225.
[15] A.I. Tsyganok, T. Tsunoda, S. Hamakawa, K. Suzuki, K. Takehira, T. Hayakawa, J. Catal. 213 (2003) 191.
[16] E. Rucksentein, Y.H. Hu, Adv. Catal. 48 (2004) 297.
[17] Y.-G. Chen, K. Tomishige, K. Yokoyama, K. Fujimoto, Appl. Catal. A: Gen. 165 (1997) 335.
[18] T. Takeguchi, S.N. Furukawa, M. Inoue, K. Eguchi, Appl. Catal. A: Gen. 240 (2003) 223.
[19] S. Damyanova, B. Pawelec, K, Arishtirova, M.V. Martinez Huerta, J.L.G. Fierro, Appl. Catal. B: Environ. 89 (2009) 149.
[20] S. Corthals, J. Van Nederkassel, J. Geboers, H. De Winne, J. Van Noyen, B. Moens, B. Sels, P. Jacobs, Catal. Today 138 (2008) 28.
[21] M. Rezaei, S.M. Alavi, S. Sahebdelfar, P. Bai, X. Liu, Z.-F. Yan, Appl. Catal. B: Environ. 77 (2008) 346.
[22] T. Osaki, T. Mori, J. Catal. 204 (2001) 89.
[23] T. Yamaguchi, Catal. Today 20 (1994) 199.
[24] B.Q. Xu, J.M. Wei, Y.T. Yu, J.L. Li, Q.M. Zhu, Topics Catal. 22 (2003) 77.
[25] J.A. Montoya, E. Romero, A. Monzón, C. Guimon, Stud. Surf. Sci. Catal. 130 (2000) 3669.
[26] X. Li, J.-S. Chang, M. Tian, S.-E. Park, Appl. Organometal. Chem. 15 (2001) 109.
[27] P. Kumar, Y. Sun, R.O. Idem, Energy Fuel. 21 (2007) 3113.
[28] P. García, A. Molina, F. Mondragón, Carbon 43 (2005) 1445.
[29] G. Stefanic, S. Music, Croat. Chem. Acta 75 (2002) 727.
[30] H.S. Roh, K.W. Jun, W.S. Dong, J.S. Chang, S.E. Park, Y.I. Joe, J. Mol. Catal. A 181 (2002) 137.
[31] J.A. Montoya, E. Romero, A. Monzón, C. Guimon, Catal. Today 63 (2000) 71.
[32] B.Q. Xu, J.M. Wei, H.Y. Wang, K.Q. Sun, Q.M. Zhu, Catal. Today 68 (2001) 217.
[33] J. Requies, M.A. Cabrero, V.L. Barrio, M.B. Güemez, J.F. Cambra, P.L. Arias, F.J. Pérez-Alonso, M. Ojeda, M.A. Peña, J.L.G. Fierro, Appl. Catal. A: Gen. 289 (2005) 214.
[34] S. Ardizzone, C.L. Bianchi, M. Fadoni, B. Vercelli, Appl. Surf. Sci. 119 (1997) 253.
[35] M.A. Aramendía, V. Borau, C. Jiménez, A. Marinas, J.M. Marinas, J.R. Ruiz, F.J. Urbano, J. Mol. Catal. A: Chem. 218 (2004) 81.
[36] Y. Hu, E. Ruckenstein, J. Catal. 163 (1996) 306.
[37] B. Bachiller, I. Rodríguez, A. Guerrero, Langmuir 14 (1998) 3556.
[38] A. Auroux, A. Gervasini, J. Phys. Chem. 94 (1990) 6371.
[39] J.D.A. Bellido, E.M. Assaf, Actas XXI Simposio Iberoamericano de catálisis, IV-1414, Málaga, España, 2008.